Available online at www.sciencedirect.com

SciVerse ScienceDirect

Acta Materialia 60 (2012) 6518–6527

Acta MATERIALIA

www.elsevier.com/locate/actamat

A DSC analysis of thermodynamic properties and solidification characteristics for binary Cu–Sn alloys

W. Zhai, W.L. Wang, D.L. Geng, B. Wei *

Department of Applied Physics, Northwestern Polytechnical University, P.O. Box 624, Youyi West Road, Xi'an 710072, People's Republic of China

Received 21 May 2012; received in revised form 7 August 2012; accepted 9 August 2012
Available online 16 September 2012

Abstract

The liquidus temperatures and enthalpies of fusion for Cu–Sn alloys are systematically measured across the whole composition range by differential scanning calorimetry (DSC). The liquidus slope vs. Sn content is derived on the basis of the measured results. The measured enthalpy of fusion is related to the Sn content by polynomial functions, which exhibit one maximum value at 55 wt.% Sn and two minimum values around 28.9 wt.% Sn and 90 wt.% Sn, respectively. The undercoolability of those liquid alloys solidifying with primary α (Cu) solid solution phase is stronger and can be further enhanced by increasing the cooling rate. However, other alloys with the preferential nucleation of intermetallic compounds display smaller undercoolings and are not influenced by cooling rate. Microstructural observations reveal that peritectic reactions can rarely be completed. With the increase in undercooling, the primary α (Cu) dendrites are refined in the peritectic Cu–22 wt.% Sn alloy. For the hyperperitectic Cu–70 wt.% Sn alloy, typical peritectic cells are formed in which the peritectic η(Cu_6Sn_5) phase has wrapped the primary ε(Cu_3Sn) phase. The DSC curves of metatectic-type Cu–Sn alloys indicate that the metatectic transformation $\gamma \rightarrow \varepsilon + L$ upon cooling is an exothermic event, and a large undercooling of 70 K is required to initiate this transformation in metatectic Cu–42.5 wt.% Sn alloy. The metatectic microstructures are characterized by (ε + η) composite structures. The η phase is mainly distributed at the grain boundaries of the coarse ε phase, but are also dispersed as small particles inside ε grains. The volume fraction of the η phase increases with the Sn content.

Keywords: Differential scanning calorimetry (DSC); Enthalpy of fusion; Undercooling; Peritectic solidification; Metatectic transformation

1. Introduction

Binary Cu–Sn alloys are applied extensively in mechanical and electronic industries because of their outstanding properties, such as high strength and thermal conductivity, excellent wear resistances and good weldability [1]. Investigations into the structures and thermodynamic properties of liquid Cu–Sn alloys, as well as their solidification characteristics, are important for the understanding of these physical and chemical properties. Therefore, many efforts have been made to explore these subjects.

The liquid structures of Cu–Sn alloys have been studied by many researchers, and the common finding is that Cu_3Sn and/or quasi-Cu_3Sn structures exist in the Cu–Sn liquids [2–7]. To determine the thermophysical properties, such as specific heat, thermal conductivity, density and liquid viscosity, of Cu–Sn alloys, Miettinen [8] developed a thermodynamic–kinetic model. The concentration and temperature dependence of surface tension for Cu–Sn liquid alloys has been theoretically investigated by Prasad and Mikula [9]. Liu et al. [10] reassessed the binary Cu–Sn phase diagram within a low temperature range, and pointed out that the solid γ phase is the DO_3-ordered structure of the β phase. By means of differential scanning calorimetry (DSC), Chen et al. [11] confirmed a temperature-induced liquid to liquid transition, which could inhibit the nucleation and growth of the primary phase during the solidification process of Cu–30 wt.% Sn alloy. Based on a single pan-thermal analysis, Rappaz and co-workers

* Corresponding author. Tel.: +86 29 88495926; fax: +86 29 88431666.
E-mail address: bwei@nwpu.edu.cn (B. Wei).

1359-6454/$36.00 © 2012 Acta Materialia Inc. Published by Elsevier Ltd. All rights reserved.
http://dx.doi.org/10.1016/j.actamat.2012.08.013

built a new heat flow model [1] to measure the solid mass fraction during solidification of Cu–Sn alloys. They also studied the directional solidification mechanism of hypo- and hyper-peritectic Cu–Sn alloys in the Cu-rich side [12] and the eutectic Sn–Cu alloys in the Sn-rich side [13,14].

Further research work is still expected on the following aspects. First, the enthalpy of fusion in the whole composition range, which is one of the fundamental thermodynamic parameters and plays an important role in computing the Gibbs free energy and determining the crystal nucleation and growth process [15], has not yet been published. Although the enthalpy of fusion for binary alloys can be roughly estimated by Neumann–Kopp's rule [16] from the values of the two pure components, this method usually results in large discrepancies [17]. Hence, the enthalpy of fusion for Cu–Sn alloys should be measured experimentally if possible. Secondly, the undercoolability of Cu–Sn alloys vs. composition is worth studying, since the solidification path and microstructural evolution are mainly dependent on undercooling. Although much work has been focused on preventing the heterogeneous nucleation of Cu–Sn alloys with various denucleation techniques [18,19], there are few reports on the intrinsic undercoolability of liquid Cu–Sn alloys vs. composition. In fact, the undercoolability also relies on the alloys themselves, and different Cu–Sn alloys may be undercooled by varying degrees even under the same external conditions. Thirdly, Cu-rich Cu–Sn alloys have been widely investigated as structural materials and Sn-rich ones have been heavily studied as lead-free solder materials, whereas little is known within the intermediate composition range from 40 to 70 wt.% Sn, as Cu–Sn alloys in this composition range have not been used for many industrial applications. In fact, an important metatectic reaction, $\gamma \rightarrow \varepsilon + L$, describing a liquid phase formation during cooling, exists in the composition range of 40–70 wt.% Sn [20]. The metatectic reaction in a nominally metatectic alloy has been studied by Lograsso and Hellawell [20], though the results have not been totally accepted by other researchers [21], and further investigation into the thermal features of the Cu–Sn metatectic reaction is required. There is also a peritectic reaction $\varepsilon + L \rightarrow \eta$ when the Sn content is greater than 58.6 wt.%. No thermal analyses or solidification microstructures involving this peritectic reaction have been reported in detail.

DSC is an efficient technique for quantitative thermal analysis [22,23]. DSC heating–cooling curves also provide essential information on the phase transition characteristics [24–26]. The objective of this work is to determine the liquidus temperatures and enthalpies of fusion for Cu–Sn alloys by DSC. Special attention is paid to the liquid undercoolability as functions of alloy composition and cooling rate. The thermal characteristics and the final solidification microstructures of typical peritectic and metatectic Cu–Sn alloys are investigated in the light of DSC calorimetric analyses.

2. Experimental

Twenty-five Cu–Sn alloys with different compositions were investigated. These are listed in Table 1 and illustrated in the binary Cu–Sn phase diagram [27] shown in Fig. 1. Each sample had a mass of about 120 mg and was prepared from high-purity elemental Cu (99.999%) and Sn (99.999%) by laser melting under the protection of argon gas.

The DSC experiments were carried out with a Netzsch DSC 404C differential scanning calorimeter. The calorimeter was calibrated with the melting points and enthalpies of fusion for high-purity In, Sn, Zn, Al, Ag, Au and Fe elements. The measuring accuracies of temperature and fusion of enthalpy are ±1 K and ±3% respectively, as verified by the measurements with the pure Cu and Sn elements. Before each DSC experiment, the alloy specimen was placed in an Al_2O_3 crucible. The chamber was evacuated and then backfilled with pure argon gas. The DSC thermal analyses were performed at different scan rates, and the maximum heating temperatures were about 150 K higher than the liquidus temperatures. Each specimen was heated, held isothermally at a predetermined temperature and then cooled at a given scan rate for 2–3 cycles while being kept in the DSC calorimeter, and the DSC profiles obtained in the last cycle were applied for further analyses.

After the DSC experiments, the alloy specimens were polished and etched with a solution of 5 g of $FeCl_3$ + 1 ml

Table 1
Thermodynamic properties of Cu–Sn alloys measured by DSC method.

Alloy composition (wt.%)	Liquidus temperature, T_L (K)	Enthalpy of fusion, ΔH_f (kJ mol^{-1})	Entropy of fusion, ΔS_f (J mol^{-1} K^{-1})
Cu–5% Sn	1332	9.934	7.46
Cu–10% Sn	1285	7.977	6.21
Cu–15% Sn	1239	6.690	5.40
Cu–22% Sn	1156	5.584	4.83
Cu–25.5% Sn	1070	5.311	4.96
Cu–27.2% Sn	1061	5.045	4.76
Cu–28.9% Sn	1043	4.797	4.60
Cu–30.6% Sn	1033	5.729	5.55
Cu–32.5% Sn	1029	6.366	6.19
Cu–38% Sn	1013	7.251	7.16
Cu–41% Sn	1000	8.006	8.01
Cu–42.5% Sn	994	8.306	8.36
Cu–46% Sn	978	9.197	9.40
Cu–50% Sn	961	9.604	9.99
Cu–55% Sn	934	9.904	10.60
Cu–58.6% Sn	913	9.379	10.27
Cu–65% Sn	889	8.740	9.83
Cu–70% Sn	871	8.030	9.22
Cu–75% Sn	847	7.515	8.87
Cu–80% Sn	811	6.587	8.12
Cu–85% Sn	776	5.620	7.24
Cu–90% Sn	727	5.424	7.46
Cu–92.4% Sn	689	5.597	8.12
Cu–95% Sn	640	6.109	9.55
Cu–97.4% Sn	585	6.674	11.41

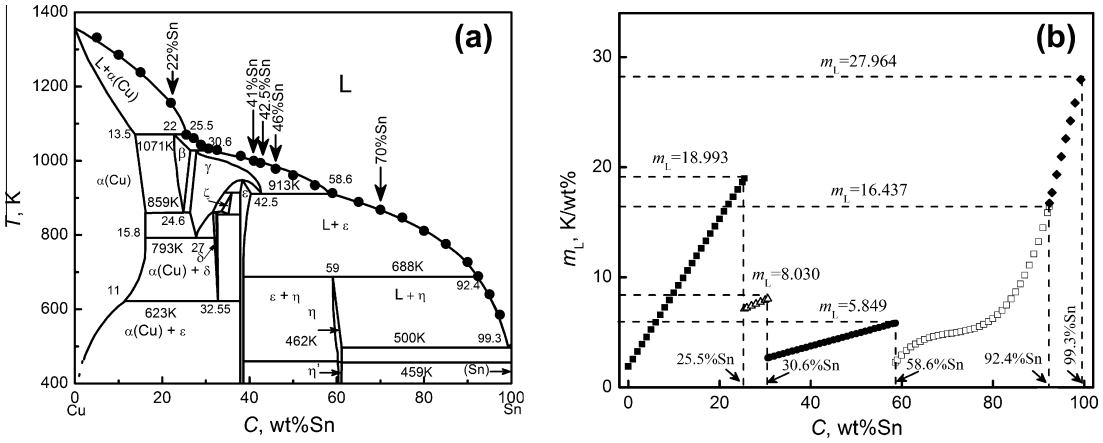

Fig. 1. Selection of alloy compositions and measured results on liquid temperatures of Cu–Sn alloys: (a) selection of alloy compositions and measured liquidus temperatures illustrated in the Cu–Sn phase diagram; (b) liquidus slope vs. Sn content.

of HCl + 99 ml of H_2O. The solidification microstructures were analyzed with an optical microscope and an FEI scanning electron microscope. The solute distribution profile was investigated with an INCA Energy 300 energy-dispersive spectrometer.

3. Results and discussion

3.1. Enthalpy and entropy of fusion

The measured liquidus temperatures of the selected alloys are marked in the Cu–Sn phase diagram shown in Fig. 1a and listed in Table 1. All the measured values agree well with the published phase diagram [27], and this verifies the accuracy of the DSC measurement. The relationship between the measured liquidus temperature T_L and the Sn content C can be fitted well by the following five functions.

In the composition range of 0–25.5 wt.% Sn, where α (Cu) is the primary solid phase:

$$T_L = 1345.30612 - 1.89656C - 0.33522C^2 \quad (1)$$

If the Sn content is within 25.5–30.6 wt.%, where the β phase solidifies preferentially from the alloy melt:

$$T_L = 1196.85 - 2.73529C - 0.08651C^2 \quad (2)$$

When the Sn content ranges from 30.6 to 58.6 wt.%, where γ is the primary solid phase:

$$T_L = 1063.44292 + 0.76777C - 0.05646C^2 \quad (3)$$

If the Sn content is in the range of 58.6–92.4 wt.%, where ε solidifies primarily:

$$T_L = -5394.30897 + 363.62365C - 7.73953C^2 + 7.252 \times 10^{-2}C^3 - 2.55825 \times 10^{-4}C^4 \quad (4)$$

Once the Sn content reaches between 92.4 and 99.3 wt.%, where the η phase is the primary solid phase:

$$T_L = -4175.80796 + 133.71677C - 0.8141C^2 \quad (5)$$

Based on Eqs. (1)–(5), the liquidus slope, defined as $m_L = -dT_L/dC$, can be calculated as follows.

If the Sn content ranges from 0 to 25.5 wt.%:

$$m_L = 1.89656 + 0.67044C \quad (6)$$

In the Sn content range from 25.5 to 30.6 wt.% Sn:

$$m_L = 2.74 + 0.17302C \quad (7)$$

When the Sn content increases from 30.6 to 58.6 wt.%:

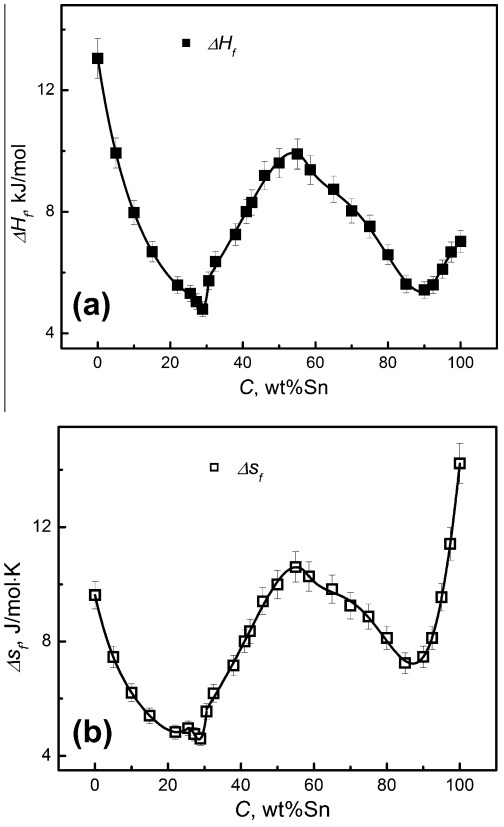

Fig. 2. Measured enthalpy and entropy of Cu–Sn alloys vs. Sn content: (a) enthalpy of fusion; (b) entropy of fusion.

$$m_L = -0.76777 + 0.11292C \quad (8)$$

If the Sn content lies between 58.6 and 92.4 wt.%:

$$m_L = -363.62365 + 15.47906C - 0.21756C^2 + 1.0233 \times 10^{-3}C^3 \quad (9)$$

In the Sn composition range from 92.4 to 99.3 wt.%:

$$m_L = -133.71667 + 1.62820C \quad (10)$$

The calculated results of the liquidus slope are illustrated in Fig. 1b. In the Sn content range of 0–25.5 wt.% Sn, the liquidus slope rises from 1.897 to 18.993 K wt.%$^{-1}$. When the Sn content increases from 25.5 to 30.6 wt.% Sn, the slope elevates slightly from 7.147 to 8.030 K wt.%$^{-1}$. If the Sn content ranges from 30.6 to 58.6 wt.%, the liquidus slope rises from 2.688 to 5.849 K wt.%$^{-1}$. In the Sn content range of 58.6–92.4 wt.%, the slope increases from 2.276 to 16.437 K wt.%$^{-1}$. On further increasing the Sn content up to 99.3 wt.%, the slope goes up remarkably, from 16.729 to 27.964 K wt.%$^{-1}$.

The enthalpy of fusion for Cu–Sn alloys vs. Sn content across the whole composition range, covering all the heat absorption from the solidus line to liquidus temperature, is determined by the solid–liquid transformation peaks during the melting process at a scan rate of 5 K min^{-1}, as summarized in Table 1 and shown in Fig. 2a. The enthalpy of fusion for Cu–Sn alloys is closely related to the primary solid phase in their solidification processes. The correlation between enthalpy of fusion and Sn content is fitted according to the five different primary solid phases in the Cu–Sn phase diagram, which are α, β, γ, ε and η phases. These polynomials are presented as follows:

In the Sn content range from 0 to 25.5 wt.%, where α (Cu) is the primary solid phase:

$$\Delta H_f(C) = 13.050688 - 0.78069964C + 3.647101 \times 10^{-2}C^2 - 1.0587136 \times 10^{-3}C^3 + 1.420977 \times 10^{-5}C^4 \quad (11)$$

When the Sn content is in the range of 25.5–30.6 wt.%, where the β phase solidifies preferentially from the alloy melt:

$$\Delta H_f(C) = -778.699 + 87.057255C - 3.2134948C^2 + 3.941923 \times 10^{-2}C^3 \quad (12)$$

If Sn is in the composition range of 30.6–58.6 wt.%, where γ is the primary solid phase:

$$\Delta H_f(C) = -20.239054 + 2.4295850C - 9.322158 \times 10^{-2}C^2 + 1.7224006 \times 10^{-3}C^3 - 1.1808138 \times 10^{-5}C^4 \quad (13)$$

In the Sn content range of 58.6–92.4 wt.%, where ε solidifies primarily:

$$\Delta H_f(C) = 406.29987 - 22.370052C^2 + 0.47184490C^2 - 4.404076 \times 10^{-3}C^3 + 1.5256999 \times 10^{-5}C^4 \quad (14)$$

Once the Sn content is higher than 92.4 wt.%, where the η phase is the primary solid phase:

$$\Delta H_f(C) = -68.7072 + 1.3690433C^2 - 6.115384 \times 10^{-3}C^3 \quad (15)$$

In the Sn content range from 0 to 25.5 wt.%, α (Cu) is the primary solid phase. The enthalpy of fusion in this region decreases monotonically with increasing Sn content. When Sn content is in the range of 25.5–30.6 wt.%, β is the corresponding primary solid phase. The enthalpy of fusion declines with increasing Sn content and reaches a minimum value around 28.9 wt.% Sn. After this, it rises slightly. For the composition range from 30.6 to 58.6 wt.% Sn, the γ phase precipitates preferentially from the alloy melt. Consequently, the enthalpy of fusion increases as the Sn content rises up to a maximum value around 55 wt.% Sn, beyond which it falls. With continuously increasing Sn content in the region of 58.6–92.4 wt.%, the ε phase becomes the primary solidifying phase. The corresponding enthalpy of fusion shows a monotonic decrease with increasing Sn content, and attains a minimum value around 90 wt.% Sn. Finally, in the residual composition range from 92.4 to 100 wt.% Sn, it is the η phase that primarily solidifies from the liquid alloy, and the enthalpy of fusion rises again with increasing Sn content.

The entropy of fusion for Cu–Sn alloys, ΔS_f, can also be calculated directly from the measured enthalpy and liquidus temperature by:

$$\Delta S_f = \Delta H_f / T_L \quad (16)$$

Fig. 2b illustrates the correlation between the entropy of fusion and alloy composition. The functional relationship between the entropy of fusion and Sn content is also fitted by five different polynomials.

In the Sn content range from 0 to 25.5 wt.%:

$$\Delta S_f = 9.6175 - 0.56964C + 3.332 \times 10^{-2}C^2 - 1.2643 \times 10^{-3}C^3 + 2.168 \times 10^{-5}C^4 \quad (17)$$

In the composition range of 25.5–30.6 wt.% Sn:

$$\Delta S_f = -699.27 + 78.319C - 2.89625C^2 + 3.5605 \times 10^{-2}C^3 \quad (18)$$

When the Sn content increases from 30.6 to 58.6 wt.%:

$$\Delta S_f = -20.348 + 2.4850C - 9.787 \times 10^{-2}C^2 + 1.836410^{-3}C^3 - 1.259 \times 10^{-5}C^3 \quad (19)$$

If the Sn content lies between 58.6 and 92.4 wt.%:

$$\Delta S_f = 604.11605 - 33.56718C + 0.7081517C^2 - 6.59973 \times 10^{-3}C^3 + 2.285572 \times 10^{-5}C^4 \quad (20)$$

Once the Sn content exceeds 92.4 wt.%:

$$\Delta S_f = 429.65353 - 9.5167C + 5.3623 \times 10^{-2}C^2 \quad (21)$$

Note that conservative error bars of ±5% are applied for all the measured and calculated points in Fig. 2. The determination of this error range is based on the fact that the measuring accuracies of temperature and fusion of enthalpy are ±1 K and ±3% for pure Cu and Sn elements.

3.2. Undercoolability of Cu–Sn alloys

We measured the undercooling ($\Delta T = T_L - T_S$) of different Cu–Sn alloys obtained in the DSC calorimeter at a scan rate of 5 K min^{-1}. Here, T_L is the measured liquidus temperature of a specific Cu–Sn alloy during heating and T_S is the initial solidification temperature upon cooling. As shown in Fig. 3a, the undercooling vs. composition can be divided into four regions, namely regions A (0–25.5 wt.% Sn), B (25.5–30.6 wt.% Sn), C (30.6–58.6 wt.% Sn) and D (58.6–97.4 wt.% Sn). In region A, α (Cu) is always the primary phase that solidifies in all the alloys, and the undercoolings are around 40–60 K. The maximum undercooling occurs around 15 wt.% Sn. The undercoolings then drop dramatically to about 8 K in the alloys of region B. The solidification processes of these alloys initiate with the nucleation of a β intermetallic compound. In contrast, in region C, where the intermetallic γ phase nucleates preferentially from all the liquid alloys, the undercoolings rise to about 15 K. In region D, where the primary phase is the ε or η phase, the undercooling remains stable around 20 K. These results suggest that the undercoolability achieved in the DSC experiments is strongly dependent on the primarily nucleating solid phases and follows the relation:

$$\Delta T_{\alpha(Cu)} > \Delta T_{\varepsilon \text{ or } \eta} > \Delta T_{\gamma} > \Delta T_{\beta} \quad (22)$$

Furthermore, five different cooling rates, 10, 20, 30, 40 and 50 K min^{-1}, were also applied to investigate their effect on the undercoolability of Cu–Sn alloys solidifying with different primary solid phases. The undercooling distribution of Cu–22 wt.% Sn, Cu–42.5 wt.% Sn and Cu–70 wt.% Sn alloys vs. cooling rate is illustrated in Fig. 3b. It is very interesting that the effect of cooling rate on the undercoolability of various Cu–Sn alloys differs remarkably. For the Cu–22 wt.% Sn alloy, with the primary α (Cu) phase, the undercooling rises linearly with the increase in cooling rate, from 40 K at a scan rate of 5 K min^{-1} to 108 K at a scan rate of 50 K min^{-1}, whereas for the latter two liquid alloys, with primary intermetallic γ and ε phases, the undercoolings exhibit no obvious changes as the cooling rate rises.

The sensitivity of undercooling on cooling rate R_c could be related to the structure differences between the liquid and primary solid phases. In the solid state of Cu–Sn alloys, the average atomic distance of Sn–Cu is much less than the distances of Cu–Cu and Sn–Sn [5]. This means that there exists a strong affinity between Sn and Cu atoms. Such a characteristic may remain when the alloy is melted, since foreign atoms get together before like atoms in the liquid Cu–Sn alloy. Bian et al. [2–4] found that the correlation radius shows an obvious change at about 1173 K in liquid Cu–Sn alloy, which proved to be induced by the forming of Cu_3Sn and quasi-Cu_3Sn structures in the liquid. Therefore, the similar structures in the liquid and solid states make the formation of solid intermetallic compounds in liquid Cu–Sn alloys easy and fast. This accounts for the strong formation ability of Cu–Sn intermetallic compounds, which is not time or cooling rate dependent. In contrast, there is a large structure difference between the liquid Cu–Sn alloy and the α (Cu) solid solution phase. The formation of α (Cu) clusters with a face-centered cubic structure needs a greater amount of recombination of Cu and Sn atoms within the liquid alloy. As a result, the nucleation of the α (Cu) phase requires a much larger driving force, and this is responsible for the strong undercoolability.

3.3. Thermal analyses and microstructure characteristics of peritectic Cu–Sn alloys

Fig. 4 shows the DSC curves of peritectic Cu–22 wt.% Sn alloy at different scanning rates. As shown in Fig. 4a, there are four endothermic events during the melting process. At a scan rate of 5 K min^{-1}, the first and second endothermic peaks at 791 and 846 K correspond to the solid transformations of α (Cu) + δ → γ and α (Cu) + γ → β, respectively. When the temperature rises to 1069 K, the solid peritectic β phase decomposes into liquid and α (Cu) phases with a very sharp endothermic peak, and the melting of the α (Cu) phase yields a relatively smooth subsequent peak. The liquidus temperature of this alloy is 1156 K. As the heating rate increases, all the transformation temperatures rise slightly. In addition to the first and

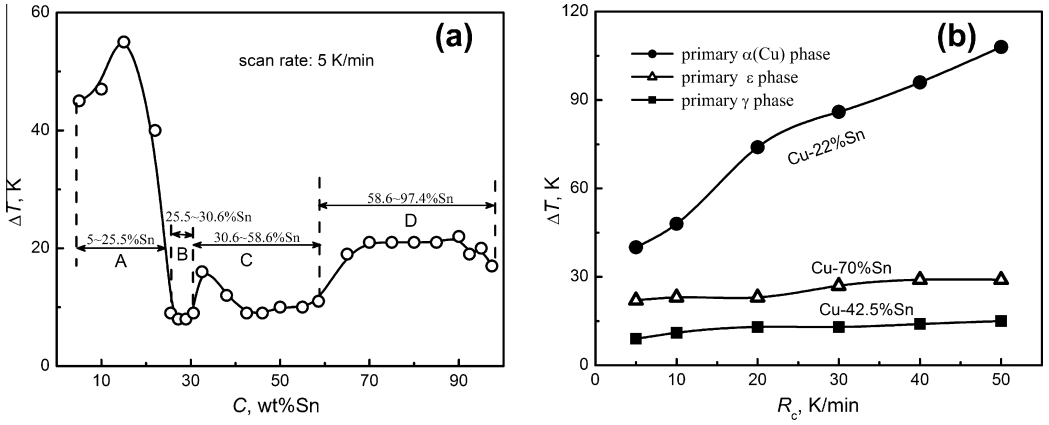

Fig. 3. Measured undercoolability of Cu–Sn alloys at 5 K min^{-1} scan rate: (a) undercooling vs. composition; (b) undercooling vs. cooling rate.

second endothermic peaks, the third and fourth ones also become increasingly overlapped due to the expansion of the neighboring peaks.

Fig. 4b displays the DSC cooling curves of Cu–22 wt.% Sn alloy with four exothermic peaks at different scan rates. At slow cooling rates (5 and 10 K min^{-1}), the exothermic peaks corresponding to the formation of primary phase and peritectic transformation are separated from each other. When the cooling rate increases to 20 K min^{-1}, the first peak becomes much sharper compared to those at 5 and 10 K min^{-1}, and the second peak starts before the first peak returns to the DSC baseline. As the cooling rate further rises to 40 K min^{-1}, the shapes of the two overlapped peaks do not change, but the maximum value of the second peak exceeds the first one, unlike that at 20 K min^{-1}. This indicates that, with the enhancement of cooling rate and undercooling, the peritectic phase competes with the primary phase, and the driving force for the peritectic phase becomes larger. When the cooling rate reaches 50 K min^{-1}, the nucleation temperature of the α (Cu) phase is 1048 K, which is even lower than the equilibrium peritectic transformation temperature 1069 K. The two peaks are nearly indistinguishable, and the first peak does not reach its maximum value until the peritectic transformation begins. The solidification interval between the nucleation of primary phase and the peritectic transition is only 5 K. This suggests that the large undercooling suppresses the growth of primary phase and promotes the peritectic transformation.

The microstructures of the Cu–22 wt.% Sn alloy solidified at different scan rates are presented in Fig. 5, and are composed of the white primary α (Cu) phase, the gray peritectic β phase and the black δ phase. According to the equilibrium Cu–Sn phase diagram [27], the entire Cu–22 wt.% Sn peritectic alloy should transform completely to β phase at the peritectic temperature. However, a large number of α (Cu) grains are reserved in the sample solidified at different scan rates. This means that the peritectic transformation occurs only to a limited extent. When the peritectic transition initially begins, the primary α (Cu) phase and liquid phase react with each other to form the β phase. As the reaction proceeds, the β phase separates the α (Cu) phase from the liquid phase gradually. In this case, the transformation process is maintained by atomic interdiffusion, so the process is very slow. As the temperature reduces, several solid transformations occur in sequence, and therefore the solidification microstructures consist of α (Cu), β and δ phases. At a cooling rate of 5 K min^{-1}, the primary α (Cu) phase is characterized by very coarse, developed dendrites, with an average length of up to 800 μm. The β phase grows around the α phase, and the (α + δ) eutectoid distributes on the matrix β phase, as shown in Fig. 5a and b. As the cooling rate increases, the crystal growth velocity also increases, resulting in an increment in the trunk length of the α (Cu) dendrites and refinement of their secondary arm spacing. As shown in Fig. 5c and d, when the alloy melt is undercooled by 108 K at a cooling rate of 50 K min^{-1}, the dendrites are much finer, and some grains appear as dendritic fragments. This is due to the recalescence effect caused by the rapid release of latent heat at a large undercooling, which would remelt the primary α (Cu) phase.

Fig. 6 presents the DSC traces of Cu–70 wt.% Sn hyperperitectic alloy at scan rates of 5, 20 and 50 K min^{-1}. There are three endothermic peaks in the melting process, which relate to the reactions $(Sn) + \eta \rightarrow L$, $\eta \rightarrow L + \varepsilon$ and $\varepsilon \rightarrow L$, respectively. At a heating rate of 5 K min^{-1}, the onset temperatures of these three transformations are 499, 680 and 871 K, and these temperatures rise slightly as the heating rate increases. The reactions take place in reverse sequence during the cooling process, and, as mentioned before, the cooling rate does not have any obvious influence on the undercooling of Cu–70 wt.% Sn liquid alloy. Fig. 7 presents the solidified microstructure of Cu–70 wt.% Sn alloy at a cooling rate of 5 K min^{-1}. The

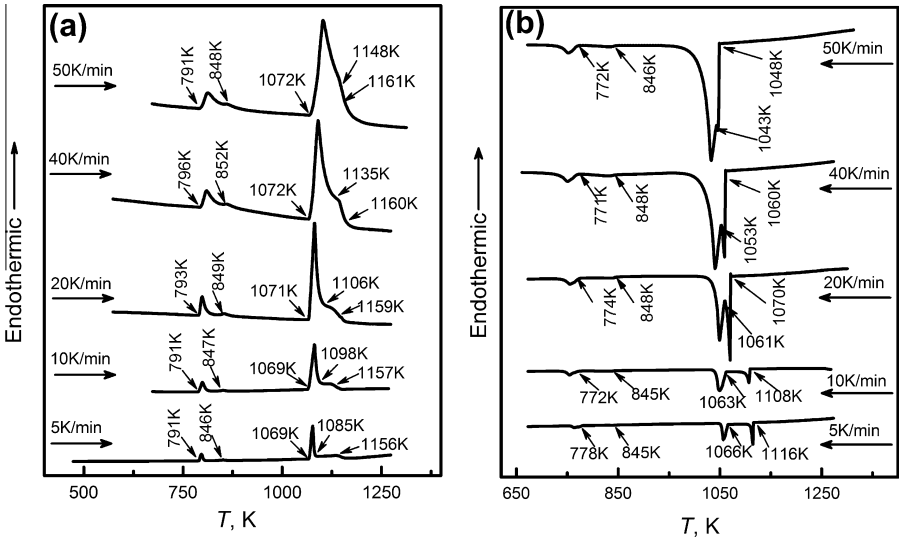

Fig. 4. DSC curves of peritectic Cu–22 wt.% Sn alloy at different scan rates: (a) melting curves; (b) cooling curves.

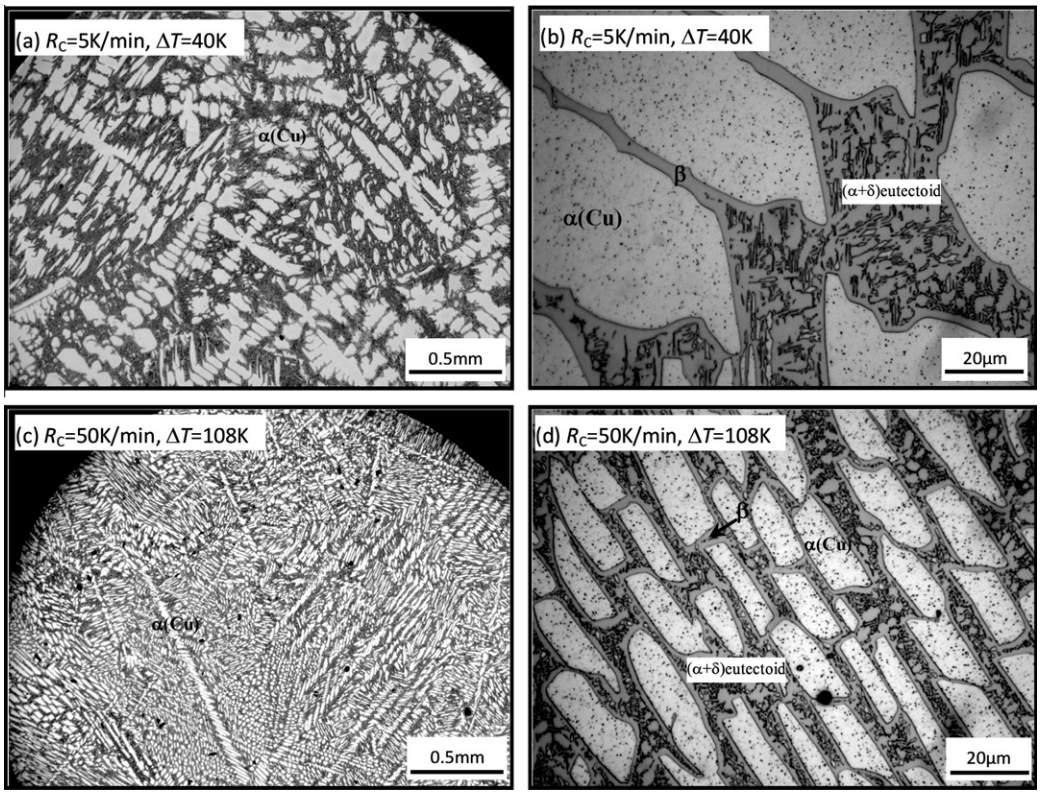

Fig. 5. Solidified microstructures of peritectic Cu–22 wt.% Sn alloy: (a) and (b) $\Delta T = 40$ K at a scan rate of 5 K min^{-1}; (c and d) $\Delta T = 108$ K at a scan rate of 50 K min^{-1}.

primary ε(Cu_3Sn) phase grows as long plates or dendrites, with an average length of 150 μm. The peritectic η(Cu_6Sn_5) phase grows by wrapping the primary ε phase to form a large number of peritectic cells. The average thickness of the η phase is 8.5 μm. Among the peritectic cells is the lamellar β(Sn) + η eutectic structure. Fig. 7c shows the EDS analysis results of the solute profile along the center axis of the peritectic cell shown in Fig. 7b. The solute Sn content in the ε phase is 40.25–40.62 wt.%, and there is 61.88–63.58 wt.% Sn in the peritectic η phase. These values are in accordance with the equilibrium value indicated in the phase diagram [27]. Since both the primary and peritectic phases are nearly stoichiometric intermetallic compounds, there are no obvious solute content variations.

The DSC cooling curves of peritectic Cu–22 wt.% Sn and Cu–70 wt.% Sn alloys at a cooling rate of 5 K min^{-1} are compared. The peritectic reaction α (Cu) + L → β in the former alloy occurs at 1066 K, which is only 3 K lower than the equilibrium transformation temperature. As a comparison, the peritectic reaction ε + L → η in the latter one takes place at 670 K, which is 10 K lower. Hence, it can be summarized that, compared with the peritectic reaction α (Cu) + L → β, ε + L → η deviates far from the equilibrium state. This result can be explained by the different structures between the primary and peritectic phases. For α (Cu) + L→ β, both the primary and peritectic phases have a cubic crystalline structure [27,28], and their lattice constants are similar. The well-matched lattices induce relative low interfacial energy between the primary and peritectic phases, so the primary phase could be the effective heterogeneous nuclei for the growth of peritectic phase. In contrast, during the peritectic reaction ε + L → η, the primary ε phase exhibits an orthorhombic structure [27,28], whereas the peritectic η phase is hexagonal [27,28]. Hence, the inter-atomic bonds in the ε phase are reconstructed to form a new structure, of the peritectic η phase. This makes it difficult for the peritectic η phase to nucleate and grow on the primary ε phase, so the peritectic reaction lags greatly. Therefore, the difference in crystalline structures of the primary and peritectic phases is the reason for the delay in the peritectic reaction of ε + L → η in Cu–70 wt.% Sn alloy at the slow scan rate of 5 K min^{-1}.

3.4. DSC curves and solidification microstructures of metatectic-type Cu–Sn alloys

Fig. 8 presents the DSC profiles of the hypometatectic Cu–41 wt.% Sn, metatectic Cu–42.5 wt.% Sn and hypermetatectic Cu–46 wt.% Sn alloys. As presented in Fig. 8a, four endothermic peaks occur during their melting processes. For the Cu–42.5 wt.% Sn alloy, the first small peak at 680 K is associated with the transformation η → ε + L. A very sharp peak then appears at 924 K, referring to the reaction ε + L → γ. This indicates that the reverse metatectic reaction during melting is an endothermic process. Following this is another endothermic peak, which relates to

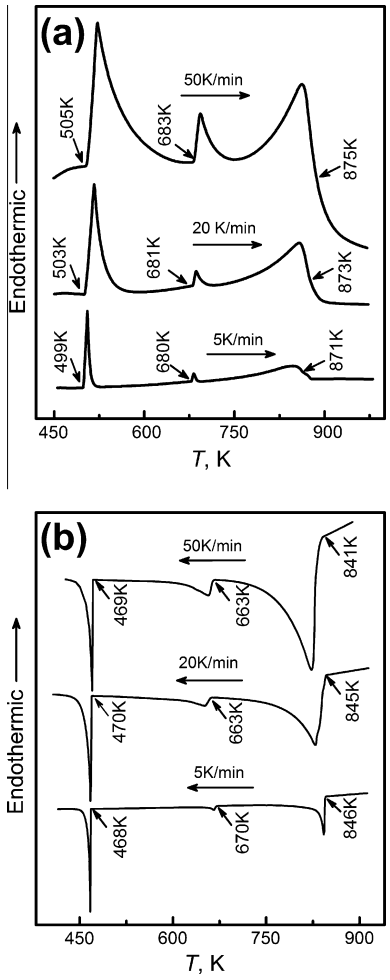

Fig. 6. DSC traces of hyperperitectic Cu–70 wt.% Sn alloy at different scan rates: (a) melting curves; (b) cooling curves.

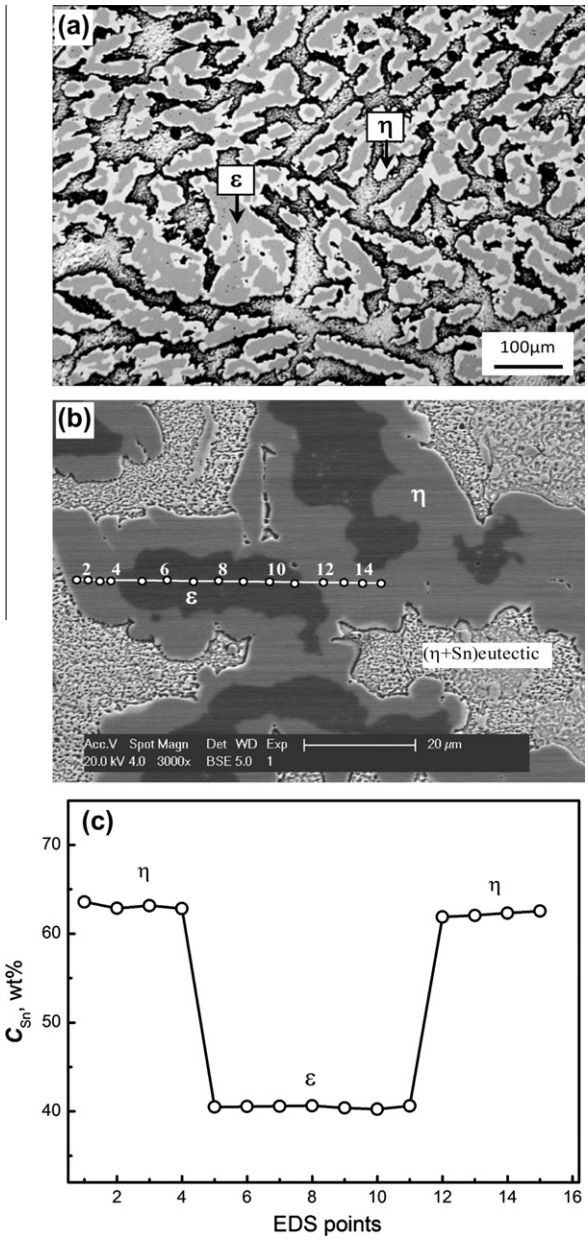

Fig. 7. Structural morphology of hyperperitectic Cu–70 wt.% Sn alloy: (a) solidified at a scanning rate of 5 K min^{-1}; (b) enlarged view of peritectic cells; (c) Sn solute distribution within the peritectic cell shown in (b).

the melting of the γ phase. The liquidus temperature of the metatectic Cu–42.5 wt.% Sn alloy is 994 K.

The melting curves of the hypometatectic Cu–41 wt.% Sn and hypermetatectic Cu–46 wt.% Sn alloys are very similar to that of the metatectic Cu–42.5 wt.% Sn alloy, except that the liquidus temperature rises slightly with increasing Sn content in the alloys. As shown in Fig. 8b, the four exothermic peaks of these metatectic-type alloys upon cooling are nearly symmetrical to the four endothermic peaks during melting, indicating that the same reaction sequence takes place in reverse order during solidification. Taking the cooling process of the metatectic Cu–42.5 wt.% Sn alloy as an example, the γ phase primarily precipitates from the liquid alloy at 983 K with a sharp exothermic peak. After this, the metatectic transformation $\gamma \rightarrow L + \varepsilon$ takes place at 854 K, which shows a large undercooling of 70 K. For the Cu–41 wt.% Sn hypometatectic and Cu–46% Sn hypermetatectic alloys, the undercoolings for this metatectic transition are 29 and 33 K, respectively. These results suggest that, like liquid to solid transformations, undercooling is required for the nucleation of the liquid phase during cooling. After the metatectic transition, the γ phase decomposes continuously until the peritectic reaction $L + \varepsilon \rightarrow \eta$ begins at 667 K, during which the liquid phase reacts with the ε phase to yield the peritectic η phase. Compared with the first and second endothermic peaks, the third one, which corresponds to this peritectic transition, is rather weak. This is due to the rather small volume fraction of liquid phase, which inhibits the peritectic reaction.

Fig. 9 displays the solidified microstructures of these metatectic-type Cu–Sn alloys, which are very similar. The microstructures are mainly composed of the dark ε(Cu_3Sn) and the white η(Cu_6Sn_5) intermetallic compounds. In all three metatectic-type alloys, the ε phase grows in the form of coarse columnar grains. When the Sn content is low,

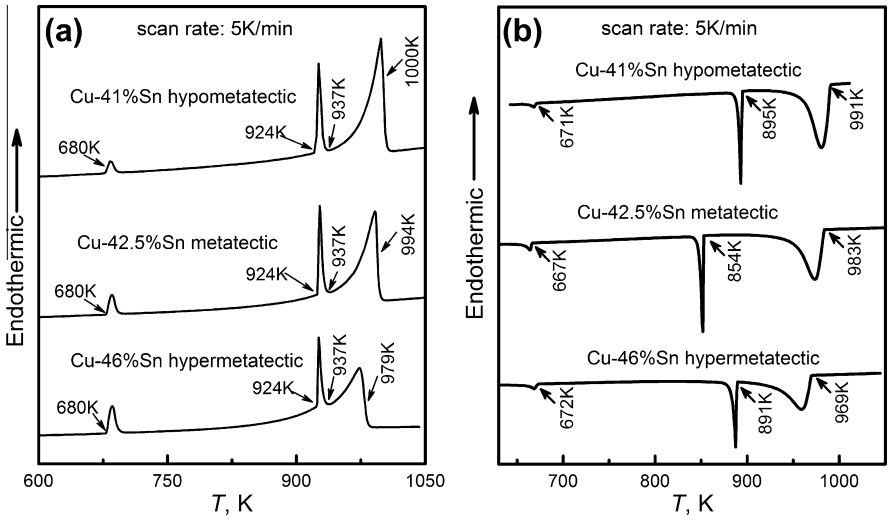

Fig. 8. Thermal analyses of metatectic-type Cu–Sn alloys: (a) melting curves; (b) cooling curves.

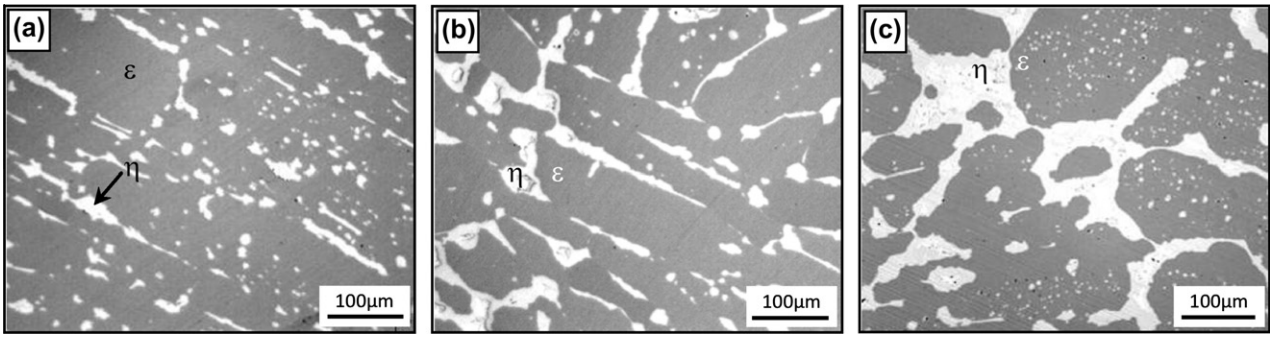

Fig. 9. Microstructures of metatectic-type Cu–Sn alloys at a cooling rate of 5 K min^{-1}: (a) hypometatectic Cu–41 wt.% Sn alloy; (b) metatectic Cu–42.5 wt.% Sn alloy; (c) hypermetatectic Cu–46 wt.% Sn alloy.

thin layers of η phase distribute at the ε phase grain boundaries, and there are a small number of global η grains inside ε grains, as presented in Fig. 9a and b. As the Sn content rises, the η grains at the boundaries of ε grains connect each other to form networks, and there is also a large number of small η particles dispersed inside the ε grains, as shown in Fig. 9c. It should be mentioned that the volume fraction of the η phase in the solidified specimens rises with increasing Sn content in these alloys. This is because the volume fraction of the liquid phase increases vs. Sn content. Consequently, the peritectic reaction could take place to a greater degree.

4. Conclusions

In summary, the liquidus temperatures and enthalpies of fusion for Cu–Sn alloys across the whole composition range are determined by DSC. The measured liquidus temperatures agree well with the published literature. The liquidus slope vs. Sn content is calculated on the basis of the measured results. The enthalpy of fusion for Cu–Sn alloys is closely related to the primary solid phase in their solidification processes. The relationship between the enthalpy of fusion and the Sn content can be fitted by polynomial functions according to the five different primary solid phases. The enthalpy of fusion reaches one maximum value around 55 wt.% Sn and displays two minimum values around 28.9 wt.% Sn and 90 wt.% Sn, respectively.

The undercoolability of liquid Cu–Sn alloys vs. alloy composition and cooling rate is investigated, and it is found that the undercooling mainly depends on the primary solid phases. At a cooling rate of 5 K min^{-1}, if the α (Cu) solid solution phase precipitates preferentially, the undercoolings of the liquid alloys range from 40 to 60 K and exhibit the maximum value around Cu–15 wt.% Sn. Furthermore, their undercoolings rise linearly with the increase in cooling rate. In contrast, the undercoolings of those liquid alloys solidifying with primary β solid phase is only around 8 K. As for other liquid alloys solidifying with primary γ, ε and η intermetallic compounds, the undercoolings are in the range of 15–20 K, and show no obvious changes even if the cooling rate rises.

The microstructural observations reveal that the peritectic reactions are rarely completed, and the solidification

microstructures of peritectic Cu–Sn alloys are usually composed of both primary and peritectic phases. In Cu–22 wt.% Sn alloy, as the undercooling increases, the primary α (Cu) phase transforms from coarse dendrites to refined grains of dendritic fragments. In contrast, peritectic cells in which the peritectic η phase enwraps the primary ε phase are formed in hyperperitectic Cu–70% Sn alloy.

The DSC thermograms of metatectic-type Cu–Sn alloys show that the metatectic transformation $\gamma \rightarrow \varepsilon + L$ upon cooling is an exothermic process, which needs a large undercooling of 70 K in the metatectic Cu–42.5% Sn alloy at a cooling rate of 5 K min^{-1}. The solidified metatectic alloys show a two-phase structure composed of ε and η intermetallic compounds. The η phase distributes at the grain boundaries of coarse ε phase, and there are also some small η particles dispersed inside the ε grains. The volume fraction of η phase increases as the Sn content rises in these alloys.

Acknowledgements

This work was supported by the National Natural Science Foundation of China (Nos. 50971105, 51201136 and 51101123) and Fundamental Research Funds of Northwestern Polytechnical University (Nos. JC20110280 and JC20120245).

References

[1] Kohler F, Campanella T, Nakanishi S, Rappaz M. Acta Mater 2008;56:1519.
[2] Zhao Y, Bian XF, Qin JY, Qin XB, Hou XX. J Non-cryst Solids 2007;353:4845.
[3] Zhao Y, Bian XF, Qin JY, Qin XB, Hou XX. Phys Lett A 2006;356:385.
[4] Qin JY, Liu H, Gu TK, Bian XF. J Phys Condens Mater 2009;21:155106.
[5] Hou JX, Sun JJ, Zhan CW, Tian XL, Chen XC. Sci China—Phys Mech Astron 2007;50:414.
[6] Adhikari D, Jha IS, Singh BP. Physica B 2010;405:1861.
[7] Pang XY, Wang SQ, Zhang L, Liu ZQ, Shang JK. J Alloys Compd 2008;466:517.
[8] Miettinen J. Comp Mater Sci 2006;36:367.
[9] Prasad LC, Mikula A. J Alloys Compd 2001;314:193.
[10] Liu XJ, Wang CP, Ohnuma I, Kainuma R, Ishida K. Metall Mater Trans 2004;35A:1641.
[11] Chen J, Zu FQ, Li XF, Ding GH, Chen HS, Zou L. Met Mater Int 2008;14:569.
[12] Kohler F, Germond L, Wagnière J-D, Rappaz M. Acta Mater 2009;57:56.
[13] Valloton M, Wagnière J-D, Rappaz M. Acta Mater 2012;60:3840.
[14] Ventura T, Terzi S, Rappaz M, Dahle AK. Acta Mater 2011;59:1651.
[15] Legg BA, Schroers J, Busch R. Acta Mater 2007;55:1109.
[16] Kopp H. Phil Trans R Soc Lond 1865;155:71.
[17] Wilde G, Gorler GP, Willnecker R. Appl Phys Lett 1996;69:2995.
[18] Mahmoudi J, Frediksson H. J Mater Sci 2000;35:4977.
[19] Battersby SE, Cochrane RF, Mullis AM. J Mater Sci 2000;35:1365.
[20] Lograsso TA, Hellawell A. Metall Trans A 1996;19A:3097.
[21] Stier M, Rettenmayr M. J Cryst Growth 2008;311:137.
[22] Witusiewicz VT, Sturz L, Hecht U, Rex S. Acta Mater 2004;52:4561.
[23] Curiotto S, Battezzati L, Johnson E, Pryds N. Acta Mater 2007;55:6642.
[24] Zarembo SN, Myers CE, Kematick RJ, Zavalij PY, Whittingham MS, Cotts EJ. J Alloys Compd 2001;329:97.
[25] Larouche D, Laroche C, Bouchard M. Acta Mater 2004;51:2161.
[26] Wang XY, Jie WQ. Acta Mater 2004;52:415.
[27] Saunders N, Miodownik AP. J Mater Sci 1987;22:629.
[28] Larsson KA, Stenberg L, Lidin S. Acta Crystallogr B 1994;50:636.